Validation and Analysis of primary atomization of turbulent liquid jet in crossflow simulations

Anirudh Asuri Mukundan, Thibaut Ménard, A. Berlemont, Jorge César C Brändle de Motta, Marcus Herrmann

ILASS-Americas 30th Annual Conference on Liquid Atomization and Spray Systems, Tempe, AZ, May 2019

Validation and Analysis of primary atomization of turbulent liquid jet in crossflow simulations

A. Asuri Mukundan[1,*], T. Ménard[1], A. Berlemont[1], J. C. B. de Motta[1], and M. Herrmann[2]
[1]CNRS UMR6614-CORIA, Rouen, France
[2]SEMTE, Arizona State University, Tempe, Arizona, USA

Abstract

This paper presents the results from direct numerical simulations of the primary atomization of a turbulent liquid jet injected into liquid crossflow. The simulations are performed for an experimentally analyzed configuration of Brown and McDonell (2006, "*Near Field Behavior of a Liquid Jet in a Crossflow*", ILASS Americas, 19th Annual Conference on Liquid Atomization and Spray Systems). The turbulent liquid jet ($q = 6.6$, Re = 14 000, We = 2178) is injected into a subsonic gaseous crossflow (Re = 570 000, We = 330). The liquid/gas interface is captured using a coupled level set volume of fluid (CLSVOF) method. The jet penetration obtained from the simulations show good agreement with the experimental correlations and also to the findings from the literature. Two breakup mechanisms are observed: column breakup mode in which waves on the windward side of the jet propagate, roll up and form bag-like structures until they breakup; and ligament breakup mode caused by the corrugations of the liquid core surface forming thin ligaments on the liquid jet sides that subsequently breakup into droplets. Analysis of the crossflow velocity component of the liquid packets from the simulation shows that a number of liquid packets exist in the domain whose velocities are same as that of the gaseous crossflow.

*Corresponding Author: anirudh.mukundan@coria.fr

Introduction

The method of atomizing liquid fuel injected into a crossflowing gas stream has been commonly employed for fuel injection in aircraft engines. With the growing number of high altitude aircrafts, it becomes increasingly interesting to study the atomization process of liquid fuel in such a configuration. The process of atomization of liquid fuel has a direct impact on its efficient combustion and on the production of pollutant emissions. With increasing stringent emission norms, it becomes imperative to study and control the atomization process based on its physics and characteristics of the liquid droplets and ligaments that are produced. Earlier studies of non-turbulent liquid atomizing jets in crossflow configurations have been reviewed by Aalburg et al [1]. More studies on the experimental work of non-turbulent liquid jets in crossflow are reported in Refs. [2, 3, 4]. A recent study by Sallam et al [5] focused on investigation of the effect of nozzle geometry on jet trajectory in supersonic conditions. The recent work of Leask et al [6] provide a systematic study examining different formulations of the injection velocity and their respective effects on momentum flux ratio of the liquid jet in crossflows. Many of these experimental works were focused on jet penetration under ambient atmospheric conditionss. Based on the experimental data, the investigators of the studies derived correlations such as that of Wu et al [7] valid in the near-injector region and Stenzler et al [8]. Such correlations depend on characteristic non-dimensional numbers such as momentum flux ratio, Weber number, and viscosity ratio between liquid fuel and liquid water.

There are many numerical studies that emulated the experimental work such as Herrmann [9, 10, 11] performing detailed numerical simulations of turbulent liquid jet in crossflow using balanced force refined level set grid (RLSG) method [12]. These studies provided the insights into the impact of finite grid spacing and density ratio on the atomization characteristics and jet dynamics. Moreover, Herrmann [9] identified two breakup mechanisms causing the atomization of liquid fuel in the simulations: column breakup mode and ligament breakup mode. Recently, Li and Soteriou [13, 14, 15] investigated the effect of increasing density, high liquid fuel viscosity and intermeditate Weber number effects on the liquid jet penetration, evolution of Sauter Mean Diameter (SMD) as a function of crossflow direction, and jet dynamics of the crossflow atomization of liquid jets. The study by Owkes et al [16] performed investigation of the effect of liquid fuel injection nozzle geometry on the atomization characteristics using large eddy simulations (LES). In this study, they used a round edged injector and sharp edged injector for injecting liquid fuel into the crossflow domain. An excellent agreement between simulations and experiments of Gopala [17] was found from their study for jet penetration for both the injector geometries. A more recent study by Ghods and Herrmann [18] performed an interesting investigation of the effect of nozzle geometry and liquid injection velocity inflow boundary conditions on the atomization characteristics. They used different inflow velocity profiles: a velocity profile from LES of in-nozzle flow and fully developed turbulent pipe flow each respectively with and without nozzle geometry for two different density ratio. They found that consistently, the results for the jet penetration using the LES of in-nozzle inflow yielded better agreement with the experimental correlation of Wu et al [7]. Furthermore, they also found that the liquid column is more deformed when using fully developed turbulent pipe inflow without nozzle geometry than when when including the nozzle geometry.

In this work, we have attempted to numerically simulate the epxerimental configuration of Brown and McDonell [2] of primary atomization of a turbulent liquid jet ($q = 6.6$, $\mathrm{Re} = 14\,000$, $\mathrm{We} = 2178$) injected into subsonic gaseous crossflow ($\mathrm{Re} = 570\,000$, $\mathrm{We} = 330$) through a direct numerical simulation (DNS) approach using a coupled level set volume of fluid (CLSVOF) method [19]. The liquid density, dynamic viscosity, and velocity are modified from the experimental conditions to keep the same non-dimensional characteristic numbers in order to have accurate results from the detailed simulations at less computational expense. Our first objective in this work is to study the atomization characteristics of the liquid jet in crossflow for the lower density ratio compared to the experimental density ratio. The second objective is to find the effect of an imposed fully developed turbulent velocity profile in the liquid phase on the atomization characteristics.

This paper is organized as follows: first, the governing equations solved in our in-house Navier-Stokes solver are presented which is followed by a brief presentation of the CLSVOF method. The computational domain and the operating conditions used in the DNS are then presented. Finaly, the results obtained from the simulations are subsequently presented and discussed.

Governing Equations

The solver used in this study is ARCHER, whose capabilities are described extensively in multiple works [19, 20, 21]. This solver is structured, par-

allel and developed for direct numerical simulations (DNS) of complex and turbulent multiphase flows with the application to study primary breakup of liquid fuel jets.

The pressure and velocity fields describing the flow are obtained by solving the incompressible Navier–Stokes equations. The following form of the Navier–Stokes equations are solved in ARCHER:

$$\boldsymbol{\nabla} \cdot \boldsymbol{u} = 0, \tag{1}$$

$$\frac{\partial \rho \boldsymbol{u}}{\partial t} + \boldsymbol{\nabla} \cdot (\rho \boldsymbol{u}\, \boldsymbol{u}) = -\boldsymbol{\nabla} P + \boldsymbol{\nabla} \cdot (2\mu \boldsymbol{D}) + \boldsymbol{B}, \tag{2}$$

where $\boldsymbol{u}$ is the velocity field, P is the pressure field, μ is dynamic viscosity, ρ is density, $\boldsymbol{D}$ is the strain rate tensor given as $\boldsymbol{D} = \frac{1}{2}(\boldsymbol{\nabla u} + (\boldsymbol{\nabla u})^T)$, and $\boldsymbol{B}$ is the sum of the body and surface tension forces. $\boldsymbol{B} = \boldsymbol{B}_\mathrm{b} + \boldsymbol{B}_\mathrm{st}$ where $\boldsymbol{B}_\mathrm{b}$ is the force due to gravity and $\boldsymbol{B}_\mathrm{st}$ is the force due to surface tension which is given as $\boldsymbol{B}_\mathrm{st} = \sigma\kappa\delta_I \boldsymbol{n}$. σ represent the surface tension coefficient, κ is the curvature of the interface computed using the liquid/gas interface unit normal $\boldsymbol{n}$ as $\kappa = -\boldsymbol{\nabla} \cdot \boldsymbol{n}$, and δ_I is the Dirac delta function centered on it. It is to be remarked that the force due to gravity is not considered in our simulations, thus, $\boldsymbol{B}_\mathrm{b} = 0$. A consistent mass and momentum flux computation [20] is employed.

A staggered variable configuration is used with central finite difference scheme for least numerical dissipation. A projection method as described in Ménard et al [19] is used for solving the Navier-Stokes equations given above. A 2^{nd} order central difference scheme is employed for discretization of the spatial derivatives to limit dissipation. However, the convection term is discretized using a 5^{th} order WENO scheme to ensure a robust behavior of the solution. A consistent mass and momentum flux computation [20] is employed. The viscous term is discretized following the method described in Sussman et al [22]. The ghost fluid method (GFM) [23] is employed for the spatial discretization of the Poisson equation for taking into account the force due to surface tension as a pressure jump. The resulting linear system is symmetric and positive definite with five diagonals is solved using a multigrid algorithm for preconditioning a conjugate gradient (CG) method [21]. The temporal derivatives in this study are discretized using a one-step forward Euler scheme.

Numerical Method

The coupled level set volume of fluid (CLSVOF) method of Ménard et al [19] is used for capturing the liquid/gas interface. The details of this method are briefly presented in the following subsections.

Level Set

The backbone of the CLSVOF method is the level set function ϕ the basis of which has been proposed by Osher and Sethian [24]. This function is a signed distance function (i.e., $\phi > 0$ in liquid phase regions and $\phi < 0$ in gas phase regions of the simulation domain) defined as the algebraic minimum distance between any point of the domain and the interface. The liquid/gas interface is then represented as the zero-level of this level set function. The advantage of this function is the ease of computation of geometric quantities pertaining to the interface. For example, the interface unit normal is computed as

$$\boldsymbol{n} = \frac{\boldsymbol{\nabla}\phi}{\|\boldsymbol{\nabla}\phi\|_2}, \tag{3}$$

and interface curvature κ is computed as

$$\kappa = -\boldsymbol{\nabla} \cdot \boldsymbol{n}. \tag{4}$$

The advection of the level set function is performed by solving the following transport equation.

$$\frac{\partial \phi}{\partial t} + \boldsymbol{u} \cdot \boldsymbol{\nabla}\phi = 0 \tag{5}$$

One of the problems that arise when solving this equation is that, due to the wide spreading and stretching of the level set in the numerical simulation domain, the level set function will no longer satisfy the condition of $\|\boldsymbol{\nabla}\phi\|_2 = 1$. Thus, a redistancing procedure [25] is required to ensure the satisfaction of this condition and keep ϕ as the algebraic distance function.

Coupling Level Set and Volume of Fluid

The combined procedure of solving Equation (5) and redistancing can create loss of mass in the numerical domain especially when reconstructing the interface for under-resolved liquid structures. In order to solve this problem, the level set method is coupled with a classical volume of fluid (VOF) method [26, 27, 28]. This coupling is performed similar to the work of Sussman and Puckett [29] the details of which are explained in Ménard et al [19]. The main differences with the CLSVOF method consist in keeping the initial re-distancing algorithm in our approach, and modifying the reconstruction technique to define the interface in a cell from the level set position.

With regards to the reconstruction of the liquid/gas interface, a PLIC method is used. Thus, a linear interface is used as an approximation of the original/reference interface. Hence, the equation of the interface in 3D is $ax + by + cz + d = 0$ where

the interface unit normal $\boldsymbol{n} = [a, b, c]^T$ and d is the shortest distance of the interface from the center of each computational cell. The components of the unit normal are determined from the level set signed distance function. In the CLSVOF method, the computation of d is performed by satisfying the volume conservation condition, i.e.,

$$\left\| F^{\text{ref}} - F^{\text{act}}(\boldsymbol{n}, d) \right\|_2 = 0, \tag{6}$$

using a Newton-Raphson method upto the machine precision. In this condition, F represents the liquid volume fraction and the superscript "ref" corresponds to the original/reference interface while "act" corresponds to the reconstructed/actual interface. The idea of solving the above equation is to perform interface reconstruction by conserving the liquid volume in the numerical simulation domain. For more details, the reader is referred to Ménard et al [19].

Computational Domain and Operating Conditions

The configuration of the liquid jet in crossflow atomization presented in this paper is the one studied experimentally by Brown and McDonell [2]. The operating conditions used in the DNS are given in Table 1. It is to be noted that the density, dynamic viscosity and velocity of the liquid phase have been modified to keep the non-dimensional numbers such as Reynolds number (Re), Weber number (We), and momentum flux ratio (q) for both phases the same as that of the experimental conditions.

The domain considered for the DNS is of the size $(-10D_j \ldots 30D_j \times -5D_j \ldots 5D_j \times -20D_j \ldots 0)$ with the liquid injector exit located at $(0, 0, 0)$. This domain is smaller than the experimental domain size of $(-77D_j \ldots 127D_j \times 0 \ldots 54D_j \times -27D_j \times 27D_j)$ [2]. The rationale behind this reduction in the domain size is to capture the atomization characteristics accurately at less computational cost. Moreover, the study by Herrmann [9] also used a reduced domain size for the same configuration to study the mesh independence on the droplet characteristics. A sketch of the DNS domain considered in this work is illustrated in Figure 1.

A uniform structured Cartesian mesh containing about 262 million cells is used for discretizing the domain resulting in a mesh resolution of $\Delta x = \Delta y = \Delta z = D_j/32$ throughout the domain. In contrast to the work of Herrmann [9], we impose a fully developed turbulent pipe flow velocity profile to the liquid injected into the domain instead of performing in-nozzle large eddy simulations (LES). Figure 2 shows the instantaneous snapshots of the three components of velocity at the injector exit plane at

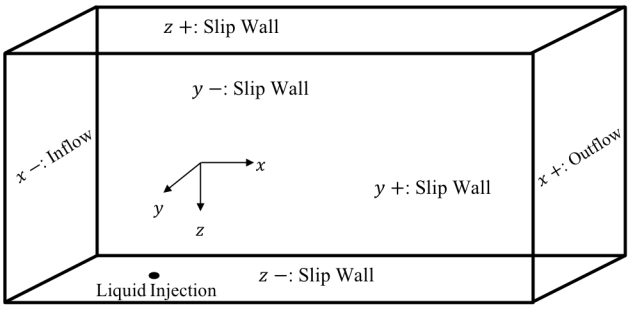

Figure 1: Illustration of computational domain used for DNS along with boundary conditions.

an instant after the first breakup event has occurred. As reported in the work of Herrmann [9], imposing a velocity profile to the liquid inlet can potentially change the droplet characteristics. The work of Ghods and Herrmann [30] studied the variation in atomization characteristics based on nozzle geometry and boundary conditions.

At $t^* = tU_j/D_j = 0$, the liquid jet is initialized in the computational domain by a cylinder of diameter D_j and height $4\Delta x$ protruding into the crossflow channel.

Results and Discussion

Figure 3 shows the time evolution of the total liquid *non-dimensionalized* mass in the domain. This mass is *non-dimensionalized* using the following expression

$$\text{Total Mass} = \frac{\sum\limits_{x,y,z} F(x, y, z)\, \Delta x \Delta y \Delta z}{D_j^3} \times \frac{\rho_j}{\rho_c}. \tag{7}$$

We can see that there is an initial increase in the total mass in the domain that is attributed to the liquid fuel injection into the domain. It can also be observed that from about $t^* = 28$, the total mass is stabilized in the domain. This means that from this time instant, a statistical steady state is reached whereby a balance exists between the injected liquid mass and the outgoing liquid mass (the liquid mass going out of the x+plane in the DNS domain, c.f. Figure 1). Since a steady state is reached for $t^* > 28$, all the statistics presented in this paper are evaluated only for $t^* > 28$ for a total of 29 non-dimensional time units. The remainder of this section is divided into qualitative and quantitative results.

Qualitative results

The averaged side view of the liquid jet in crossflow for $t^* > 28$ is shown in Figure 4. In order to be

Table 1: Operating conditions and non-dimensional numbers

Quantity	**Unit**	**Experiment**	**Simulation**
Jet diameter (D_j)	[mm]	1.3	1.3
Jet density (ρ_j)	[kg/m^3]	1000	12.25
Jet velocity (U_j)	[m/s]	10.83	97.84
Jet viscosity (μ_j)	[kg/ms]	1.0×10^{-3}	1.11×10^{-4}
Surface tension (σ)	[N/m]	0.07	0.07
Crossflow gas density (ρ_c)	[kg/m^3]	1.225	1.225
Crossflow gas velocity (u_c)	[m/s]	120.4	120.4
Crossflow viscosity (μ_c)	[kg/ms]	1.82×10^{-5}	1.82×10^{-5}
Momentum flux ratio (q)	[-]	6.6	6.6
Jet Weber number (We$_j$)	[-]	2178	2178
Jet Reynolds number (Re$_j$)	[-]	14079	14079
Crossflow Weber number (We$_c$)	[-]	330	330
Crossflow Reynolds number (Re$_c$)	[-]	5.7×10^5	5.7×10^5

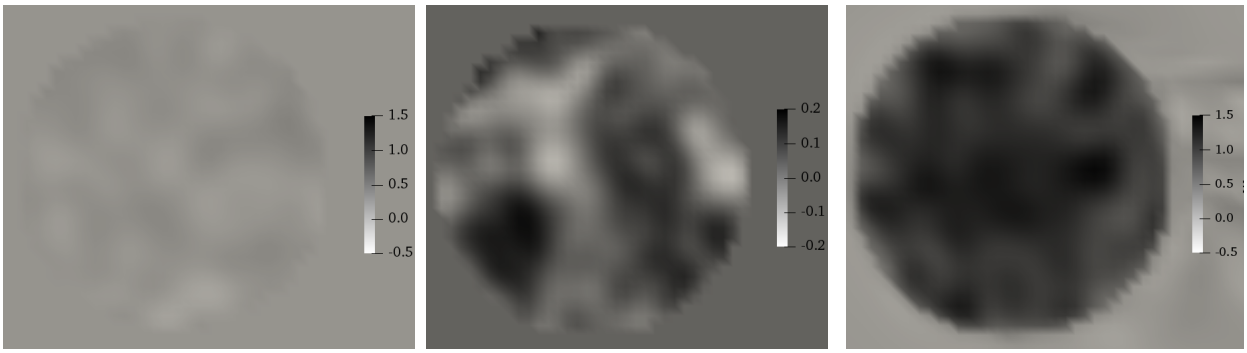

(a) u/u_j (b) v/u_j (c) w/u_j

Figure 2: Instantaneous snapshots of the velocity at the injector exit plane. The velocity component values in the legend in each figure has been *non-dimensionalized* using jet injection velocity.

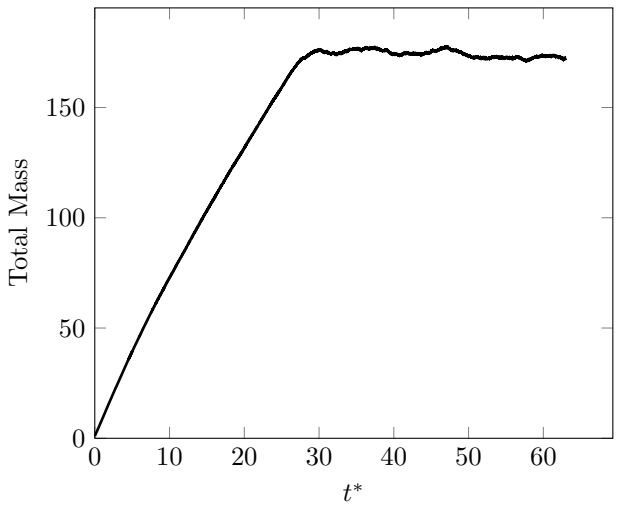

Figure 3: Temporal evolution of total non-dimensionalized liquid mass in the DNS domain.

consistent in post-processing the results, the averaging is performed directly on the images. The difference between averaging the data and averaging the visual images is out of the scope of this paper and is currently considered as further steps to be taken after this work. In this figure, the jet penetration and bending is compared against two experimentally fit correlations: first, the correlation by Wu et al [7] given by the expression

$$\frac{y}{D_j} = 1.37 \left(\frac{x}{D_j} \right)^{1/2}, \tag{8}$$

and second, the expression given by Stenzler et al [8]

$$\frac{y}{D_j} = 2.63 q^{0.442} \left(\frac{x}{D_j} \right)^{0.39} \mathrm{We}_c^{-0.088} \left(\frac{\mu_j^{\mathrm{experi}}}{\mu_{\mathrm{H_2O}}} \right)^{-0.027}. \tag{9}$$

In this expression, the term μ_j^{experi} refers to the dynamic viscosity of the liquid used in the experiments.

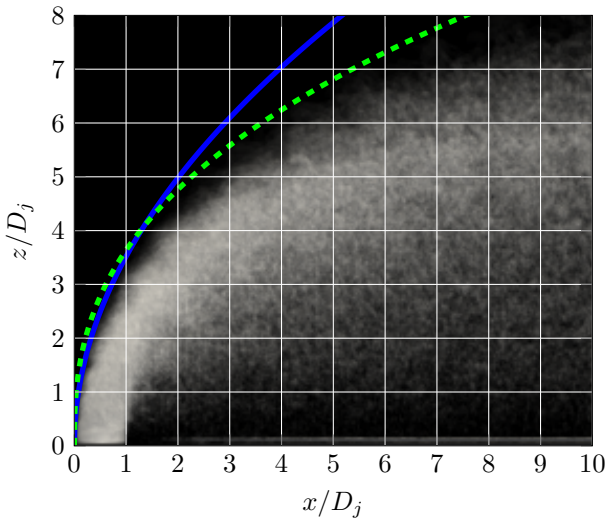

Figure 4: Averaged side view of the liquid jet in crossflow with experimental curve fit. Wu et al [7] (——) (upper curve) and Stenzler et al [8] (- - -) (lower curve)

In the experiments of Brown and McDonell [2] liquid water was used. Since this work emulates the experimental work, we thus have, $\mu_j^{\text{experi}}/\mu_{\text{H}_2\text{O}} = 1$ in the above mentioned Stenzler correlation (c.f. Equation (9)). It is to be noted that the correlation from Wu et al [7] (c.f. Equation (8)) is valid only in the near-injectory region. Analyzing this figure, we can find that our simulation results qualitatively matches better with the correlation by Stenzler et al [8] shown by the green dashed line as the lower curve than the correlation by Wu et al [7] shown by the blue solid line as the upper curve. Such an observation has been found in both experimental [2] and simulation works [9, 11]. Thus, we find that our simulation results agree well with the experimental correlations and also with the findings from the literature.

Figures 5 and 6 shows the snapshots of the visualization of the atomizing liquid jet at different time instants. Two main mechanisms of atomization can be observed from these visualization images. First, the instability waves are formed predominantly on the windward side of the liquid jet that roll-up along the jet axis forming a bag-like structure which then breaks up into droplets. Such a mechanism of atomization is similar to the column breakup mode which generates small droplets of the size of the thickness of the bag-like structures. The second breakup mechanism is the ligament breakup wherein corrugations in the liquid jet surface are stretched out into ligaments at the side of the liquid jet (as seen in Figure 6). Such a breakup mechanism produces medium and large droplets that are of the size of the ligaments.

Quantitative results

In order to understand the atomization characteristics and further develop secondary breakup models, quantitative results extracted from the results of the DNS are presented in this section. In this section, result from a preliminary quantitative analysis is presented. To this end, statistics about the liquid packets in the domain are extracted. In order to uniquely count the liquid packets, we set up a control volume that is of length $6\Delta x$ along the x direction in the farthest x+plane in the downstream direction. The liquid packets that fall within this $6\Delta x \times L_y \times L_z$ domain at any time instant are considered to be going out of the domain or are about to go out of the domain the next sampling time step. Here, $L_y = 10D_j$ and $L_z = 20D_j$ represent the lengths of the domain along y and z directions.

Figure 7 shows the discrete number based frequency distribution of crossflow velocity component of the liquid packets in the domain. The information about the velocity distribution is pertinent for the development of models for the primary atomization processes that involve injection of drops along projected mean liquid core paths with a given velocity [31]. This frequency distribution has been generated by binning the liquid packets into 20 equally sized bins between the minimum and maximum velocities along the crossflow direction. This velocity component is non-dimensionalized using the crossflow gas velocity as the relevant velocity scale in this direction. From this plot, we can observe that velocity of numerous liquid structures are same as that of gaseous crossflow, i.e., these structures are following the gaseous crossflow streamlines. The shift in the peak of this distribution from the value 1 could be caused due to the blockage of the gaseous flow by the jet.

Conclusions

The results from direct numerical simulations (DNS) of an experimentally analyzed liquid jet in subsonic crossflow configuration have been presented. The domain has been reduced in size in comparison to the experiments to have accurate results at relatively less computational expense. All the non-dimensional characteristic numbers for the flow are maintained the same as in the experiment except the artificial reduction of the density ratio to study its effect on the jet penetration, breakup mechanism, and atomization characteristics.

The jet penetration has been studied by averaging all the side view visualisation images of the cross-

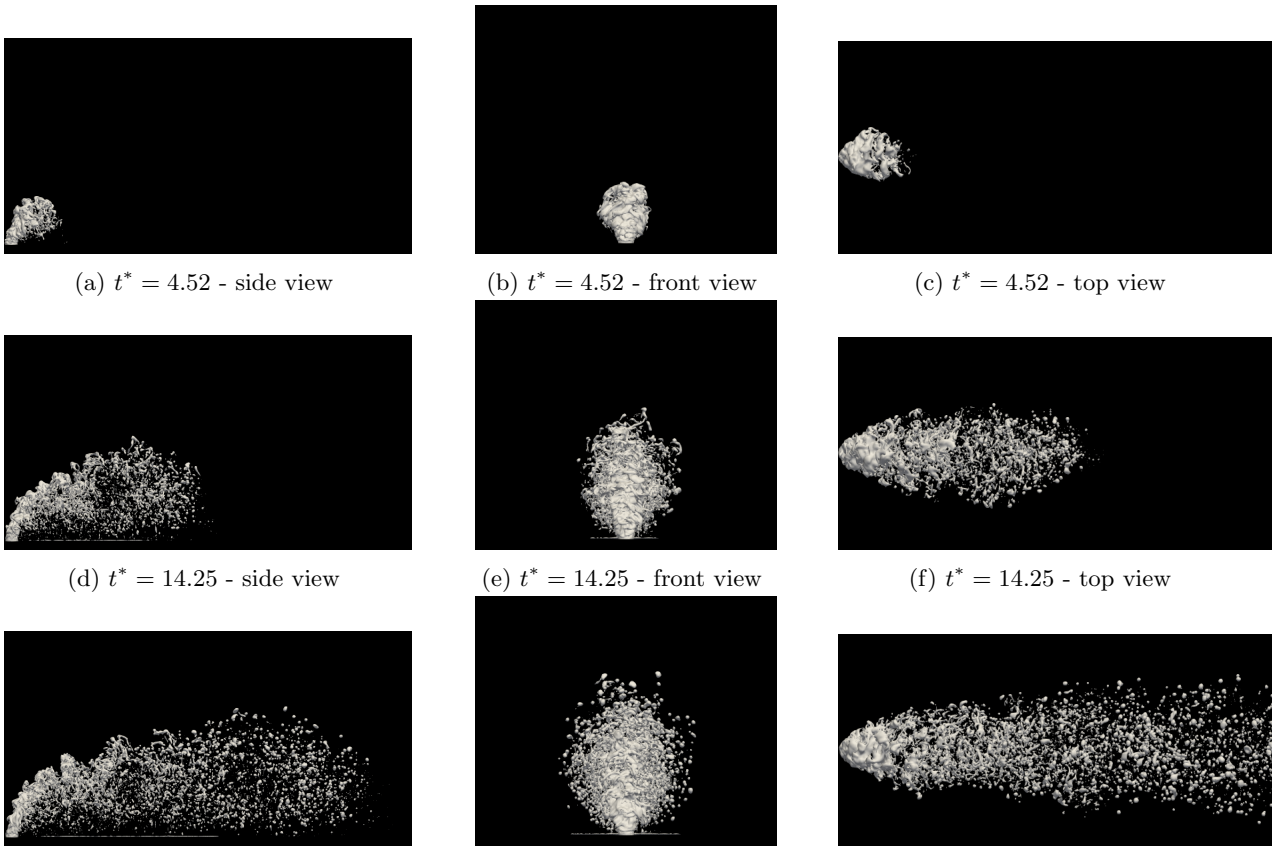

(a) $t^* = 4.52$ - side view (b) $t^* = 4.52$ - front view (c) $t^* = 4.52$ - top view

(d) $t^* = 14.25$ - side view (e) $t^* = 14.25$ - front view (f) $t^* = 14.25$ - top view

(g) $t^* = 24.65$ - side view (h) $t^* = 24.65$ - front view (i) $t^* = 24.65$ - top view

Figure 5: Side view (left column), front view (middle column), and top view (right column) of the atomization of liquid jet in crossflow

flow liquid jet and comparing with the experimental correlations. The jet penetration has been found to be consistent with the experimental correlations and findings from the literature. Preliminary qualitative analysis of the jet shows that the atomization is governed by two main mechanisms: first, a column breakup-like mechanism in which there is generation of instability waves in the windward side of the liquid core that roll up and continue to grow along the axis of the jet thereby forming bag-like structures leading to formation of droplets; and second, a ligament breakup mechanism wherein the corrugations in the liquid jet surface are stretched out into ligaments on the side of the liquid jet near the exit of the injector. These ligaments get further stretched and eventually break up into droplets.

An initial quantitative analysis of the crossflow velocity component of the liquid packets in the simulation domain has been made. To that end, the discrete number based frequency distribution of the crossflow component of the velocity has been computed. This distribution revealed that numerous liquid packets exist in the domain with the velocity about the same as that of the gas phase crossflow.

In the future, employment of multiple mesh resolutions with varying density and viscosity ratio to investigate the mesh independence, impact of density and viscosity ratio on the atomization characteristics and jet dynamics are under consideration.

Acknowledgements

The funding for this project from the European Union's Horizon 2020 research and innovation programme under the Marie Skłodowska-Curie grant agreement N° 675676 is gratefully acknowledged. The computing time at CRIANN (Centre Régional Informatique et d'Applications Numériques de Normandie) under the scientific project No. 2003008 is also gratefully acknowledged.

References

[1] C. Aalburg, B. van Leer, G. M. Faeth, and K. A. Sallam. *Atomization and Sprays*, 2005.

Figure 6: Visualization of liquid jet in crossflow at $t^* = 32$.

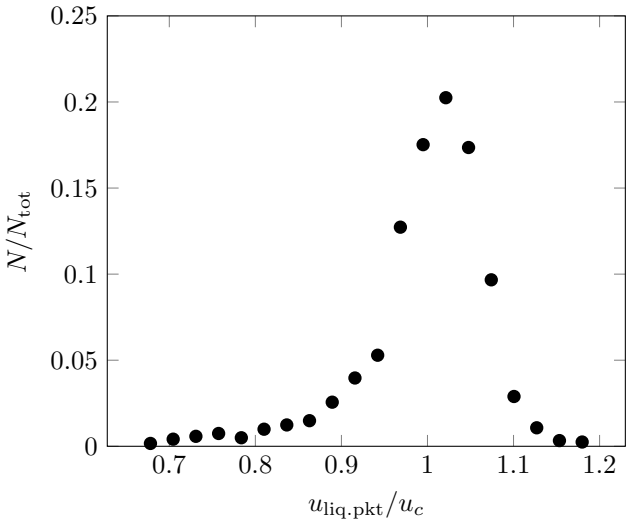

Figure 7: Discrete number based frequency distribution of crossflow velocity component of liquid packets in the simulation domain.

[2] C. T. Brown and V. G. McDonell. *ILASS Americas, 19th Annual Conference on Liquid Atomization and Spray Systems, Toronto, Canada*, 2006.

[3] S. Freitag and C. Hassa. *ILASS – Europe 2008, 21st Annual Conference on Liquid Atomization and Spray Systems, Como Lake, Italy, 8-10 September*, number ILASS08-12-1, 2008.

[4] C.-L. Ng, R. Sankarakrishnan, and K. A. Sallam. *International Journal of Multiphase Flow*, 34(8):241–259, March 2008.

[5] K. A. Sallam, K.-C. Lin, S. D. Hammack, and C. D. Carter. *ICLASS 2018, 14th Triennial International Conference on Liquid Atomization and Spray Systems, Chicago, IL, USA, July 22-26*, 2018.

[6] S. B. Lease, V. G. McDonell, and S. Samuelsen. *Atomization and Sprays*, 28(7):599–620, 2018.

[7] P. K. Wu, K. A. Kirkendall, R O. Fuler, and A. S. Nejad. *Journal of Propulsion and Power*, 13(1):64–73, January 1997.

[8] J. N. Stenzler, J. G. Lee, D. A. Santavicca, and W. Lee. *Atomization and Sprays*, 2006.

[9] M. Herrmann. *Journal of Computational Physics*, 229:745–759, 2010.

[10] M. Herrmann. *Proceedings of the Combustion Institute*, 33(2):2079–2088, 2011.

[11] M. Herrmann, M. Arienti, and M. C. Soteriou. *Journal of Engineering for Gas Turbines and Power*, 2011.

[12] M. Herrmann. *Journal of Computational Physics*, 227:2674–2706, 2008.

[13] X. Li and M. C. Soteriou. *Physics of Fluids*, 28(8):082101–1–082101–35, 2016.

[14] X. Li, H. Gao, and M. C. Soteriou. *Physics of Fluids*, 29:082103–, 2017.

[15] X. Li and M. C. Soteriou. *International Journal of Multiphase Flow*, 104:214–232, July 2018.

[16] M. Owkes, M. G. Pai, and O. Desjardins. *52nd Aerospace Sciences Meeting*, 2014.

[17] Y. Gopala. PhD thesis, Georgia Institute of Technology, 2012.

[18] S. Ghods and M. Herrmann. *ILASS-Americas 25th Annual Conference on Liquid Atomization and Spray Systems, Pittsburgh, PA, May 2013*, 2013.

[19] T. Ménard, S. Tanguy, and A. Berlemont. *International Journal of Multiphase Flow*, 33(5):510–524, 2007.

[20] G. Vaudor, T. Ménard, W. Aniszewski, M. Doring, and A. Berlemont. *Computers & Fluids*, 152:204–216, 2017.

[21] S. Tanguy and A. Berlemont. *International Journal of Multiphase Flow*, 31:1015–1035, 2005.

[22] M. Sussman, K. M. Smith, M. Y. Hussaini, M. Ohta, and R. Zhi-Wei. *Journal of Computational Physics*, 221(2):469–505, 2007.

[23] R. Fedkiw, T. Aslam, B. Merriman, and S. Osher. *Journal of Computational Physics*, 152(2):457–492, July 1999.

[24] S. Osher and J. A. Sethian. *Journal of Computational Physics*, 79(1):12–49, November 1988.

[25] M. Sussman, E. Fatemi, P. Smereka, and S. Osher. *Computers & Fluids*, 27(5–6):663–680, June 1998.

[26] E. Aulisa, S. Manservisi, R. Scardovelli, and S. Zaleski. *Journal of Computational Physics*, 192(1):355–364, 2003.

[27] J. Hernández, J. López, P. Gómez, C. Zanzi, and F. Faura. *International Journal for Numerical Methods in Fluids*, 58:897–921, 2008.

[28] J. López, C. Zanzi, P. Gómez, F. Faura, and J. Hernández. *International Journal for Numerical Methods in Fluids*, 58(8):923–944, 2008.

[29] M. Sussman and E. G. Puckett. *Journal of Computational Physics*, 162,:301–337, 2000.

[30] S. Ghods and M. Herrmann. A consistent rescaled momentum transport method for simulating large density ratio incompressible multiphase flows using level set methods. 2013.

[31] M. Behzad, A. Mashayek, and N. Ashgriz. *ILASS Americas 22nd Annual Conference on Liquid Atomization and Spray Systems, Cincinnati, OH, USA, May 16-19, 2010*, number ILASS2010-112, May 2010.